Modification of anatase TiO_2(001) surface electronic structure by Au impurity

E. Mete [a,*], O. Gülseren [b], and Ş. Ellialtıoğlu [c]
[a] *Department of Physics, Balıkesir University, Çağış Campus, Balıkesir 10145, Turkey*
[b] *Department of Physics, Bilkent University, Ankara 06800, Turkey*
[c] *Department of Physics, Middle East Technical University, Ankara 06531, Turkey*
(Dated: July 3, 2009)

We have used density functional theory calculations based on the projector augmented wave method to investigate the electronic structure of Au-incorporated anatase TiO_2(001) surface. Due to the coordination with several level oxygens, Au atoms can be encapsulated inside TiO_2 slab. Au is adsorbed over the surface Ti–O bond, so called the bridge site on anatase TiO_2(001)–1×1 surface. However, for 0.25 ML coverage, Au atoms energetically prefer to stay at 0.64 Å above the midpoint of the two surface oxygens which is significantly closer to the surface layer. When implanted inside the slab for full coverage, Au forms parallel metallic wires inside TiO_2 lattice where interlayer distances increase due to local segregation. Au brings half-filled impurity states into the band gap leading to metallization, in addition to other filled surface and impurity bands within the gap. These Au-driven Fermi-level-pinning gap states are close to, or even in some cases inside, the conduction band of the host slab. On the other hand, if Au is substituted for the surface Ti atom, Fermi level falls lower in the gap closer to the valence band top.

PACS numbers: 73.20.Hb, 68.43.Bc

arXiv:0907.0599v1 [cond-mat.str-el] 3 Jul 2009

I. INTRODUCTION

Lately, titania (TiO_2) has received an increased attention since it is considered to be promising for cost-effective photovoltaic applications. However, high reactivity of TiO_2 under only UV light bears a great disadvantage which reduces the quantum efficiency so that pure TiO_2 is not alone sufficient for a practical system application.[1,2,3,4,5]

McFarland and Tang[6], in a recent work, proposed an Au/TiO_2/Ti multilayer photovoltaic device on which photon absorption occurs in the deposited dye molecules while electron–hole pairs are created upon light illumination inside the semiconductor for the conventional solid-state solar cells. This ultrathin metal–semiconductor junction Schottky diode has driven a particular attention to gold–titania interface[7].

Gold has been proposed to enhance the catalytic activity of anatase TiO_2.[8,9] Au incorporated anatase-based nanocatalysts have been synthesized for device applications.[10,11,12] Moreover, diffusion of gold into anatase polymorph of titania has also been reported.[13]

The anatase phase of titanium dioxide, although being less stable than the rutile polymorph, is catalytically more active[14,15,16]. In this sense, the surface properties are of major importance. There are several studies on the topological and electronic structure of the single crystals of anatase TiO_2(001) surface[17,18,19,20]. In this paper, we investigated the reconstructive effect of various types of Au incorporation in the anatase substrate and the role of such an impurity on the electronic structure of TiO_2(001). We considered Au in and on the surface at quarter and full monolayer (ML) concentrations including Au(Ti) substitutional cases as well as gold dimer adsorption on the surface. We have discussed their thermodynamic stabilities for various experimental environments.

II. METHOD

The total energy density functional theory (DFT) calculations have been performed within the generalized gradient approximation (GGA) for the exchange–correlation effects via Perdew–Burke–Ernzerhof (PBE96) functional[21], using plane-wave basis sets and the projector augmented waves (PAW) method[22,23] as implemented in the Vienna Ab-initio Simulation Package (VASP)[24].

Anatase TiO_2(001) stoichiometric surface has been modeled as a symmetrical slab which constitutes 6 TiO_2 layers in a supercell with a vacuum region of at least 13 Å. A TiO_2 layer consists of 3 atomic planes in which bridging oxygen atoms are out of the level Ti-plane. Our choice regarding the number of layers represent one of the thickest slab models among the other theoretical studies[17,18,19,20]. Moreover, for Au implantation deeper than the fourth atomic plane we used 8-TiO_2-layer slab model to avoid any interaction between the Au impurities within the same supercell which are implanted from the bottom and from the top surfaces.

For the gold incorporated surface models we kept ions, only in the central TiO_2 layer, fixed to their bulk positions because the forces on these remain to be insignificantly small in all of the calculations. We employed a conjugate-gradients algorithm to compute the electronic ground state based on the minimization of the total energy subject to a convergence tolerance of 0.1 meV. Geometry optimization has been performed, subsequently,

*Corresponding author: e-mail: emete@balikesir.edu.tr

by the reduction of the quantum force on each of the unconstrained ions to less than 10 meV/Å.

Single particle wavefunctions have been expanded in terms of plane waves up to a cut-off energy value of 400 eV. The Brillouin zone (BZ) integrations have been carried out over 32 and 5 special k-points sampled in the irreducible wedge for 1×1 and 2×2 surfaces, respectively. We did not impose any symmetry in our surface calculations.

In thermodynamic equilibrium, the most stable surface composition, that is entirely surrounded by a thermal bath at temperature T under a given pressure p, minimizes the surface Gibbs free energy $\gamma(T,p)$ (GFE).[25,26,27,28] Therefore, relative stability of the phases can be expressed in terms of the difference $\Delta\gamma(T,p)$ in the GFE of impure surface structures and relaxed clean surface, as,

$$\Delta\gamma(T,p) = \frac{1}{A}\Big\{G_{\mathrm{Au/TiO_2}}(T,p,\Delta n_{\mathrm{Ti}},\Delta n_{\mathrm{Au}}) - G_{\mathrm{TiO_2}}(T,p) - \Delta n_{\mathrm{Ti}}\mu_{\mathrm{Ti}}(T,p) - \Delta n_{\mathrm{Au}}\mu_{\mathrm{Au}}(T,p)\Big\},$$

where $G_{\mathrm{Au/TiO_2}}$ and $G_{\mathrm{TiO_2}}$ are the GFEs of the Au incorporated and reference clean TiO_2 surface slabs, respectively. A is the corresponding unit cell area, also functioning as normalization for different stoichiometries. As the name suggests, Δn is the difference in the number of atoms from that of the reference surface while μ denotes the chemical potential for the referring species. A negative $\Delta\gamma$ value indicates a more stable structure relative to the clean TiO_2 surface. Positive values, on the other hand, give the relative formation energy that is required to assemble the corresponding composition.

GFE, in general, is defined by, $G = U + pV - TS$. One can omit pV term in comparison to the surface energy for the pressures, p, under consideration as well as the TS term since the contribution from the entropy, S, is negligible. Therefore, it can be approximately expressed only by the internal energy U. If one also neglects the ionic vibrational contributions, U will be equal to the total energy $E_{\mathrm{total}}(N,V)$ obtained by the DFT slab calculations.

Thermodynamic equilibrium is established when the chemical potential of a given atomic species becomes equal in all phases that come into contact with each other. In particular, we assume that the surface structures are in equilibrium with the anatase TiO_2 bulk so that $\mu_{\mathrm{Ti}} + 2\mu_{\mathrm{O}} = \mu_{\mathrm{TiO_2}}$. Moreover, the reference energies at the most stable elemental phases of Ti and Au set the upper bounds for their corresponding chemical potentials. For instance, the maximum value of μ_{Ti} can be accessed in the *hcp* Ti bulk solid phase. Otherwise, the bulk phase would be unstable with respect to precipitation of bulk Ti. Similarly, μ_{Au} can not be above the chemical potential of *ccp* gold bulk. Molecular oxygen defines the upper boundary for μ_{O} so that $\mu_{\mathrm{O}} = \frac{1}{2}E_{\mathrm{O_2}}$ which corresponds to an O–rich experimental environment, therefore, defining the minimum value of μ_{Ti} through the thermodynamic equilibrium condition, $\mu_{\mathrm{Ti}} + 2\mu_{\mathrm{O}} = \mu_{\mathrm{TiO_2}}$.

III. RESULTS AND DISCUSSION

We systematically studied Au impurities on and inside the anatase TiO_2(001) stoichiometric surface. The role of such an incorporation on the electronic properties of anatase surface has been investigated by examining adsorptional, substitutional, and interstitial impurities at quarter and full coverages. For these concentrations, we considered gold ions in the subsurface at the interstitial cavities up to a depth of the fifth atomic plane, and also substituted them for Ti ions up to the third Ti plane.

The topological structure and the electronic properties of the bare anatase TiO_2(001) has been discussed in detail elsewhere[29]. Fig. 1 shows the optimized geometries and corresponding electronic structures of Au–TiO_2 combined systems for 1×1 surface. The first two panels to the left show the side views of the geometric structures along [100] and [010] directions. In addition, relevant electronic structures are presented next to these geometries at each row representing a distinct impurity case.

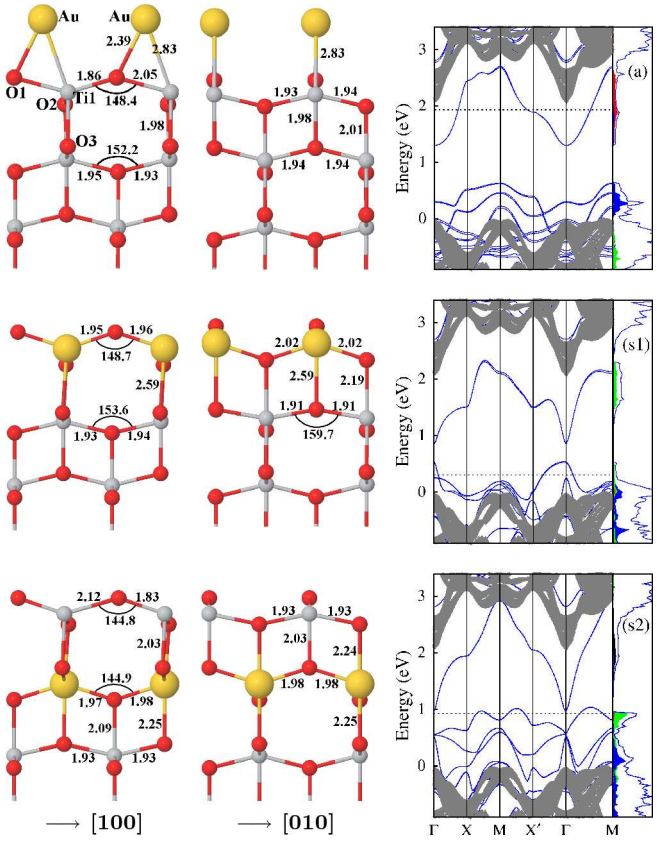

FIG. 1: (color online) The geometric and electronic structures of a–1 × 1 (first row), s1–1 × 1 (second row), and s2–1 × 1 (last row), for the Au/TiO_2(001)-1×1 systems. Big lightgray (yellow) balls represent gold. Small dark (red) and bright (gray) balls denote oxygen and titanium atoms, respectively. Bond angles and bond lengths are given in degrees and angstroms, respectively. Energy bands and DOS structures are described in detail in the corresponding subsections.

Each ion is labeled with respect to the atomic plane, that it belongs to, for each of species separately. For instance, an oxygen at the second oxygen atomic layer is labeled as O2. Furthermore, bulk termination gives rise to undercoordinated ions by breaking the axial bonds over the surface. As a result, O1 and Ti1 become twofold and fivefold coordinated, thus, also referred as O2c and Ti5c, respectively.

A. Au/TiO_2(001)-(1×1)

1. Adsorptional case: a–1×1

Au-adsorptional case, that the first row of Fig. 1 refers to, has been obtained by relaxing all possible initial configurations in which Au comes into contact with the active sites on the support surface. Truly, in this resultant geometry, Au relaxes to a bridge position on O1 and Ti1 that reflects the maximum interaction between the Au adsorbate and the surface. At this minimum energy position O1–Au–Ti1 angle becomes 45.4° with Au–O1 and Au–Ti1 bond distances being 2.39 and 2.83 Å, respectively. The reconstructive effect of the adsorbate on the lattice remains negligibly small at the subsurface layers. Au adsorption at 1ML coverage adapts an ideal-like TiO_2 atomic arrangement by saturating the dangling bonds. Yet, the symmetry breaking in the Ti1–O1 bonds which stems from the relaxation of the clean surface, is still not lifted as bond lengths read 2.05 and 1.86 Å. The structural parameters as well as some other physical entities related to electronic properties such as the surface work function and Fermi energy relative to bulk valence band maximum (VBM) are presented in Table I.

Au adsorbate brings a two-dimensional impurity state in the gap closer to the conduction band (CB). Fermi level passes through the saddle point at X′ of this band corresponding to a logarithmic singularity in the site-projected (local) density of states (LDOS). This half-filled Fermi-level-pinning state, therefore, leads to metallization. The reactivity of the O1 site is higher than that of Ti1, which is also apparent from the LDOS presented on the rightmost panel of the corresponding electronic band structure in Fig 1. A group of four occupied defect states lie distinctly below the Fermi energy derived from the valence band (VB) possessing dominant O1 character. The contribution of Ti1 to the total DOS around the Fermi energy is very weak.

2. Substitutional case: s1–1×1

The most noticeable effect of Au substitution for surface Ti (Ti1) at 1×1 structure, also referred as s1–1×1, is that the distance between the top and the second TiO_2 layer increases substantially. For instance, the Ti1–O3 axial bond length of 1.96 Å at the clean surface extends to 2.59 Å for Au–O3. In addition to the increase in the interlayer distance, this extension also gets the Ti2–O3–Ti2 angle to enlarge from 152.0° to 159.7° at the second TiO_2 layer. Moreover, Au–O1 equatorial bonds along [100] at the surface layer become almost equal being 1.95 and 1.96 Å as shown in the second row of Fig. 1.

Unlike to that of the adsorptional case, Au–Ti1 substitution drives Fermi energy to fall lower in the gap closer to the valence band top. Because of the partially-occupied nature of this state which is populated by Au, O1, and chiefly by O2, the combined system goes into the metallic regime. The upper lying unoccupied defect state, which takes up a big portion of the gap to the energies above the Fermi level as a result of the strong dispersion, shows dominant Au and O2 contribution.

3. Substitutional case: s2–1×1

The optimized geometry presented in Fig. 1(s2) for the second substitutional case (s2–1×1) has been obtained by relaxing an initial configuration which was formed by replacing Ti2 with Au in the bare 8-TiO_2(001)-layer slab model. Au impurity sits below the surface in the second TiO_2 layer having extended interlayer distances, similar to s1–1×1 case, of 2.24 and 2.25 Å with the top and the third layers, respectively. On the other hand, Ti1–O1 bond lengths remain to be nonequivalent with values of 2.12 and 1.83 Å making a Ti1–O1–Ti1 angle of 144.8°.

Subsurface substitutional gold sets the Fermi level at 0.93 eV above the valence band maximum (VBM) pinned by a strongly dispersed empty defect state, of ∼2 eV wide, which descends from the CB. The second band below, with a width of about 0.5 eV is partially filled causing metallization of the system. This band is degenerate with a third band of similar width at Γ point, and all these three states are symmetrical with respect to M point along $\overline{\Gamma XMX'\Gamma}$. The unoccupied first band is originating mainly from the Au–O4 and Au–Au interactions. The half-occupied second one shows dominant O2 and relatively weaker O4 character. Third band has an LDOS peak stemming from O3. The fourth band in the gap which crosses the third along most of $\overline{XMX'}$ is due to the clean surface (see Fig. 2(a) in Ref. [18]). The LDOS for the surface oxygen (O1) disperses over VB similar to that of s1–1×1 implying a charge transfer to subsurface cation sites. This results in a work function of 6.06 eV. We have also considered Au substitution for Ti3 (not shown). The band structure for s3–1×1 has common characteristics with that of s2–1×1. The first and second bands are very similar, third is no longer degenerate with the second at Γ, and fourth, the surface state, is pushed down towards the VB, and is also symmetric with respect to M. In quest of finding a trend we checked the band structures for Au substituted even deeper, namely for Ti5 (s5–1×1) and also considered a case for bulk substitution. Comparison of these series of cases, Au for Ti1 to bulk Ti, band structures projected to the same surface Brillouin zone shows that the second

TABLE I: Calculated electronic and structural parameters for Au–TiO_2(001) anatase system: work function, position of the Fermi energy relative to bulk valence band maximum, Au-depth relative to surface oxygens, Au–O and Au–Ti distances for each model labeled in compliance with Fig. 1, Fig. 2, and Fig. 3.

Model	W(eV)	E_F(eV)	h_{Au}Å	d_{Au-O}Å	d_{Au-Ti}Å
a–1×1	5.45	1.93	2.14	2.39(O1)	2.83(Ti1)
s1–1×1	6.37	0.31	−0.51	1.95(O1), 2.03(O2)	3.51(Ti2)
s2–1×1	6.06	0.93	−3.22	2.24(O2), 1.98(O3, O4), 2.25(O5)	3.23(Ti1), 3.28(Ti3)
a–2×2	5.02	2.02	1.94	2.20(O1)	2.68(Ti1)
b–2×2	4.29	2.60	0.64	2.06(O1), 2.73(O2)	3.06(Ti1)
c–2×2	4.33	2.59	−2.71	3.17(O2), 2.09(O3), 2.50(O4)	2.85(Ti1), 2.77(Ti2)
d–2×2	4.49	2.57	−3.40	2.46(O3), 2.05(O4), 3.13(O5), 2.74(O6)	2.80(Ti2), 2.94(Ti3)
e–2×2	4.47	2.58	−5.24	3.11(O4), 2.06(O5), 2.49(O6), 3.55(O7)	2.93(Ti2), 2.78(Ti3)
s1–2×2	6.80	0.31	−0.27	2.01(O1), 2.03(O2)	3.37(Ti2)
s2–2×2	6.66	0.58	−3.18	2.07(O2), 2.59(O3), 2.02(O4), 2.03(O5)	3.45(Ti1), 3.18(Ti3)
aa–2×2	6.28	1.04	1.57	2.32(Au1–O1), 2.07(Au2–O1)	2.66(Au1–Ti1), 2.67(Au2–Ti1)

and third bands continue to repel each other, while E_F passes through the second defect band as before.

4. Interstitials at 1×1

For the interstitial case at 1×1 surface, strong metal–metal interaction distorts the local lattice structure drastically due to shortened Au–Au distance of 3.76 Å. This causes a local segregation that leads to the formation of parallel metallic Au wires along [010] inside TiO_2 lattice where interlayer distances further increase (from ∼2.02 to 3.89 Å).

B. Au/TiO_2(001)-(2×2)

1. Adsorptional case: a–2×2

Similar to the case for the 1ML coverage, single Au adsorbate at the 2×2 surface is twofold coordinated with O1 and Ti1 at the bridge position over the Ti1–O1 bond as shown in Fig. 2(a). Au promotes the nearest-neighbor Ti1 upward elongating the Ti1–O3 bond from a clean surface value of 1.96 to 2.02 Å. It also interacts strongly with the nearest O1 which is elevated up leading to a significant increase in the Ti1–O1 bondlength, from 2.16 to 2.40 Å, over which Au stays at the minimum energy position. As a result, O1–Ti1–O1 angle gets wider by 4° compared to the value at the clean surface. Quarter ML Au adsorption yields significant differences in the atomic positions from those of the 1ML coverage. For instance, Au–Ti1 and Au–O1 bond lengths become shorter (2.68 and 2.20 Å) than the values (2.83 and 2.39 Å) for 1ML coverage, respectively. This can be explained by the increased charge transfer between the impurity and the support surface due to much weaker Au–Au impurity interaction at 1/4 ML coverage.

For a–2×2 case, energy gap region is characterized by weakly dispersing six defect states as shown in Fig. 2(a). The one lying just below the CB that is half filled by simple electron counting drives the combined system into metallic state. This Au–O1 driven state is flat along $\overline{\mathrm{JK}}$ and almost flat along $\overline{\mathrm{J'\Gamma}}$ and therefore quasi-one dimensional in nature as seen also in LDOS. The next defect state that lies 1.56 eV below the Fermi energy at Γ being also quite flat, especially along $\overline{\mathrm{JKJ'}}$, has mainly O2 character. The remaining four states come up slightly above the VBM with many crossings originating mainly from Au–O1 and Au–Ti1 interactions.

2. Adsorptional case: b–2×2

In the second adsorptional model, namely b–2×2, Au relaxes into a very symmetrical position, 0.64 Å above the midpoint between two O1 ions. It forms two and four equidistant bonds with those O1 ions and with Ti1s that read 2.06 Å for the former and 3.06 Å for the latter, respectively. This isotropic coordination with two nearest neighbor O1s and with four surface 'Ti's get Ti1–O3 bonds to be aligned parallel to [001]. Hence, each of the Ti1–O1 bonds become equal to 2.10 Å in length making and angle of Ti1–O1–Ti1 angle of 137.6°. On the other hand, two Ti2–O2 bonds that are coplanar with Au remain to be slightly skewed with congruent angles of 3.6° each.

Fermi level falls into the CB by a resonant defect state causing metallization for the electronic structure presented in Fig. 2(b). Two flat going occupied defect states lie about 0.5 and 0.9 eV above VBM. The higher one of these bands carries dominant O1 character, whereas the lower one originates from Au–O1 interaction with larger Au mixing, and has some O2 contribution as well.

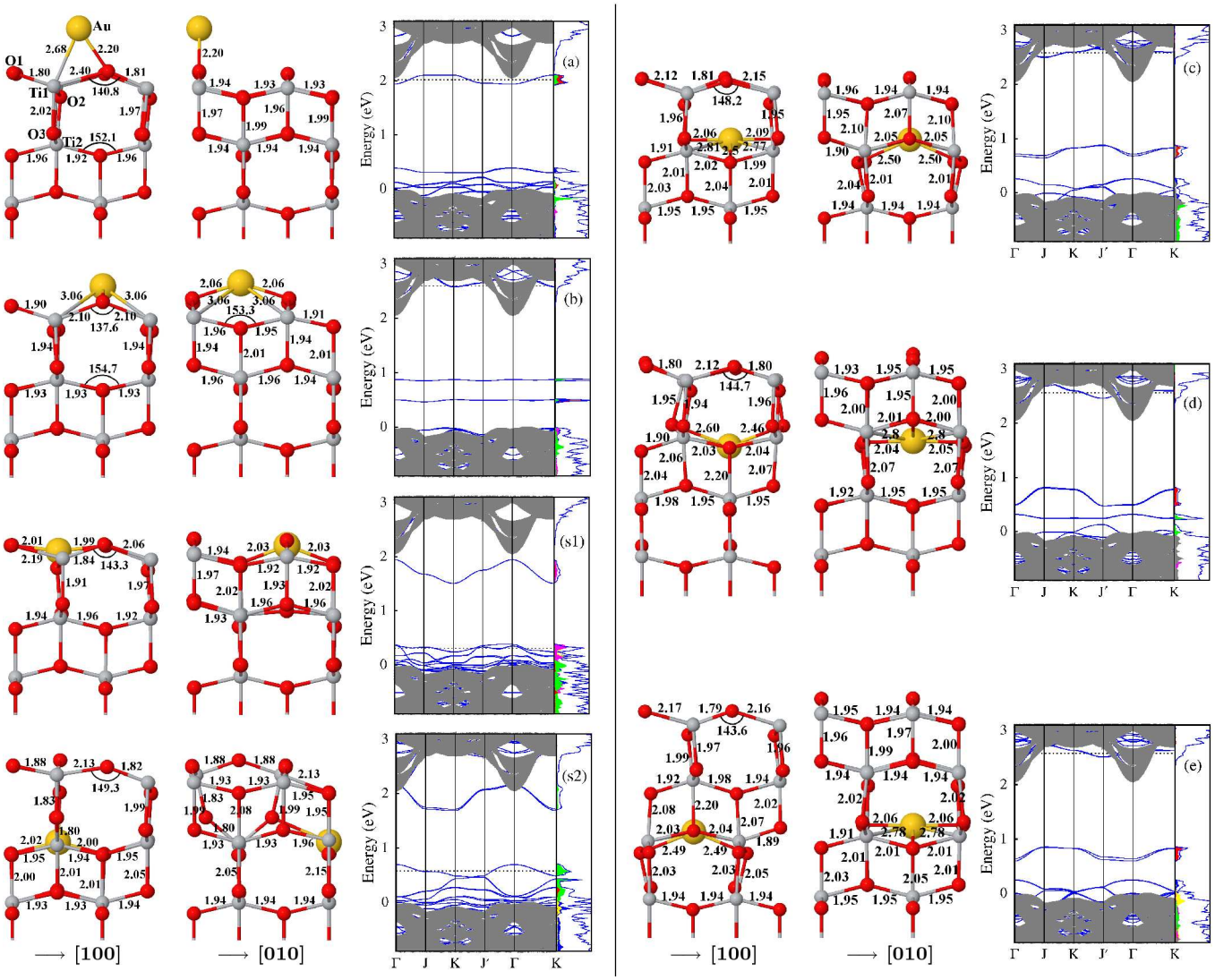

FIG. 2: Geometric and electronic structures of $Au/TiO_2(001)$-2×2 systems for the adsorptional, substitutional, and interstitial gold incorporations. Label for each case, is given in the DOS panel, should read as, e.g., a–2 × 2 for the first row, and so on. Naming convention for the atoms follow those of Fig. 1. The bond lengths and angles are given in angstroms and in degrees, respectively.

3. *Substitutional case: s1–2×2*

When substituted for surface titanium as shown in Fig. 2(s1), Au relaxes into a position, 0.38 Å above the original Ti1 lattice point, where it forms two Au–O1 bonds with slightly unequal lengths of 1.99 and 2.01 Å. It is also twofold coordinated to two nearest-neighbor O2s at a distance of 2.03 Å away from each. The inequivalency in the Ti–O1 bond lengths still remains being 1.84 and 2.06 Å over the undercoordinated surface oxygen row along [100] next to the row in which Au substituted. Moreover, Au–O3 separation elongates to 2.65 Å which can be attributed to Au attaining a nominal charge state that weakens the charge transfer from Au to O3. Resulting bond length of Ti2 with this O3 shortens to 1.85 Å while the other Ti2–O3 distances are all 1.96 Å.

A stack of surface bands disperse over an energy range of 0.33 eV with intercrossings just above VBM. The highest of those is half occupied setting the Fermi energy at 0.31 eV relative to bulk valence band top. Therefore, combined system has been predicted to show metallic behavior. The two sharp LDOS peaks at and just below the Fermi level in Fig. 2(s1) are mainly due to O1 which is bonded to Au. The rather lower part of those surface states, on the other hand, originate from undercoordinated O1s which are away from Au site. An empty defect state falls into the gap region at around 2 eV at Γ below CB having a minimum at K. This band has two saddle points at J and J′ which are not at the same energy because of the unequal Au–O1 bondlengths along [100]. Corresponding LDOS peaks come out as a result

of excess anti-bonding charge localized around gold.

4. Substitutional case: s2–2×2

Au substitution for Ti2 causes local disturbances on the nearby O3s as a result of the excess charge embedded by and localized around the impurity site. Equatorial Au–O3 bonds on (100) plane extend to 2.59 Å leading to a significant dislocation of O3s from their lattice positions. This subsurface reconstruction induces stress on Ti1–O3 interaction that flips up Ti1–O2 bonds. Then, the displaced O2 levels itself with O1 atomic plane as shown in Fig. 2(s2). On the other hand, subtle atomic rearrangements have been observed upon Au substitution for Ti2 over the planes perpendicular to [010] direction. In this structure, Ti1–O1 bonds are still unequal (2.13 and 1.82 Å) making a Ti1–O1–Ti1 angle of 149.3°. Au substitution for a third layer Ti cation, namely s3–2×2, dislocates the nearby O3s in the same way as s2–2×2 does. This suggests that Au–Ti replacement for deeper lying cations will cause similar local reconstruction.

The electronic structure of s2–2×2 model in Fig. 2(s2) have similar characteristics with that of s1–2×2. Both of them has an unoccupied defect state arising chiefly from Au impurity. However, the one for the s2 case lies higher and so partly inside CB at around Γ. It is slightly dispersed along $\overline{\mathrm{JK}}$ and $\overline{\mathrm{J'\Gamma}}$ causing the band to be a quasi-1D band as opposed to the quasi-2D band of s1 case. This also shows itself in their LDOS structures. An O2 driven half-filled defect state having a maximum at Γ has been hived off from the lower lying group of surface-like bands. Therefore, Fermi level is at 0.58 eV with respect to bulk valence band top. This is related to the surface oxygen, O2, that is bonded to Au. The next band down is also of O2 character, however, it gets additional contributions from the surface oxygen, O2, raised to the level of O1s, as well. In comparison with those of s1–2×2, the stack of surface bands disperse over a relatively higher energy range of 0.47 eV just above VBM. They are due mainly to axial Au–O2 interaction. LDOS also shows contributions to bands slightly below VBM primarily from surface oxygens. As in the 1×1 case we have examined the deeper Au substitutions for up to bulk Ti which lead the half-filled defect state to move about 1 eV upward closer to the empty band in the gap.

5. Interstitials at 2×2

Au can be encapsulated at the interstitial cavities in the subsurface layers starting from the fourth atomic layer for 2×2 surface as opposed to 1×1. The first three possible structures are presented in Fig. 2(c)–(e). As common to all of them, Au relaxes into the midpoint between the two level oxygens where it also establishes equidistant coordination with four nearest neighbor 'Ti's that lie at the closest Ti atomic plane. Au interstitial causes local disturbances such that two second nearest-neighbor oxygens at the preceding or succeeding O layers get slightly repelled out from their bulk lattice positions due to the induced stress incorporated by the excess charge at the impurity site. Au implantation to the internal cavities can not help lifting the symmetry breaking in the Ti1–O1 bond distances that exists in the case of the bare anatase surface.

The interstitial Au impurities in TiO_2(001) surface, corresponding to Fig. 2(c)–(e), show similar electronic characteristics since they represent equivalent local environments. For all of them, Fermi level falls in CB due to an impurity driven state that lies in the energy gap region along $\overline{\mathrm{JKJ'}}$ and partly along the $\overline{\mathrm{K\Gamma}}$ segment. The fully occupied quasi-1D defect state just below 1 eV disperses in accordance with the spatial alignment of Au–O coordination. Therefore, its maximum at J′ for c–2×2 and at J for d–2×2 and e–2×2, (doubly) alternates with Au–O bond orientation. Lower lying nearly flat state in case–d is due primarily to O2 oxygens at the surface. For the cases c and especially e, the stack of bands just above VBM are very similar to those of the clean surface (see Fig. 2(a) in Ref. [18]), because the region of disturbance due to the interstitial Au is away from the first TiO_2 layer for these cases, and for cases with deeper interstitials.

IV. BADER ANALYSIS

We analyzed the electronic charge density using the atom in molecule (AIM) theory with a grid-based algorithm[30]. Computational Bader charge results for near surface Ti and O atoms, and also for the Au impurity, are presented in Table II for the combined systems as well as for the clean surface. For Au–TiO_2(001) structures, atomic charge states are provided for O and Ti ions that are closest to gold site in order to better describe the local disturbance of the electronic density, posed by the impurity.

The non-ionic nature of Ti–O bonding in TiO_2 stoichiometry, due to below-nominal charge states of Ti cations and O anions, has been previously shown[29,31]. Bulk ions accumulate $Q_{\mathrm{O}} = -1.33e$ and $Q_{\mathrm{Ti}} = +2.66e$ Bader charges while these values are slightly lower for the corresponding surface layer species, being $Q_{\mathrm{O1}} = -1.26e$ and $Q_{\mathrm{Ti1}} = +2.61e$, due to bulk termination.

Bader charge results presented in Table II for the impurity neighboring ions demonstrate the local disturbance of the electronic density. The fluctuation in the charge density around the cation sites remains minimal upon Au incorporation. For interstitial and adsorptional cases, gold seems to weakly bound to the lattice because of a limited charge transfer from Au to nearby oxygens. We obtained relatively smaller deviations in the charge states of deeper lying atoms implying a weaker contribution to surface electronic properties. When gold is substituted for Ti cations it induces deviation in the electronic density also around the second nearest neighbor oxygens

owing to its spatially wider spread wavefunction. For instance, Au–Ti1 substitution in s1–1×1 charges the third layer oxygen to $Q_{O3} = -1.18e$ that is smaller than its reference value of $Q_{O3} = -1.33e$ at the clean surface.

In comparison with their reference values at the clean surface, a lower amount of charge accumulation at the anions around the impurity site has been obtained for all Au–TiO_2(001) structures in Table II. This elicits a weak polarization in the covalency between gold and oxygen at this surface. The Au–O and Ti–O interaction strengths can be compared based on the charge transfers in between. The electron depletion from Ti to O is clearly much larger than that from Au to O suggesting that Ti–O bond is stronger.

A. Au dimer on 2×2

The weakness of Au–O bond polarization, in and on TiO_2 surface, compared to that of Ti–O opens the possibility of an important interaction between two adjacent Au atoms. Clearly, Au driven impurity bands disperse relatively stronger when they are incorporated to 1×1 surface unit cell in Fig 1. Therefore, we considered all possible adsorption configurations of Au dimer on 2×2 surface in order to investigate the effect of Au–Au interaction on the electronic structure of the combined system. Fig. 3 shows the minimum energy Au dimer structure on the anatase TiO_2(001)-2×2 surface. This is obtained from an initial configuration in which one Au atom is placed over the Ti1–O1 bond in bridge position and the other one is located over the next Ti1–O1 bond on the back Ti–O–Ti row. They are attracted to each other due to Au-Au interaction. Relatively speaking with respect to the structure shown in left-top of Fig 3, as they come

TABLE II: Bader charge analysis of Au–TiO_2(001) anatase systems. Atom labels follow Fig. 1, Fig. 2, and Fig. 3. The values represent the valence charge states for lattice atoms that are closest to Au impurity site.

Model	O1	O2	O3	Ti1	Ti2	Au
clean	−1.26	−1.34	−1.33	+2.61	+2.64	—
a–1×1	−1.20	−1.34	−1.33	+2.58	+2.64	−0.03
s1–1×1	−0.70	−0.85	−1.18	—	+2.64	+1.38
s2–1×1	−1.24	−1.17	−0.94	+2.58	—	+1.54
a–2×2	−1.15	−1.34	−1.32	+2.55	+2.65	−0.04
b–2×2	−1.18	−1.35	−1.33	+2.57	+2.62	+0.34
c–2×2	−1.26	−1.33	−1.24	+2.55	+2.56	+0.34
d–2×2	−1.25	−1.34	−1.30	+2.60	+2.56	+0.34
e–2×2	−1.26	−1.34	−1.34	+2.60	+2.58	+0.38
s1–2×2	−0.95	−1.11	−1.26	—	+2.63	+1.39
s2–2×2	−1.20	−1.03	−1.27	+2.63	—	+1.32
aa–2×2 (Au1)	−1.23	−1.35	−1.32	+2.56	+2.64	−0.07
aa–2×2 (Au2)	−1.12	−1.35	−1.33	+2.54	+2.64	+0.05

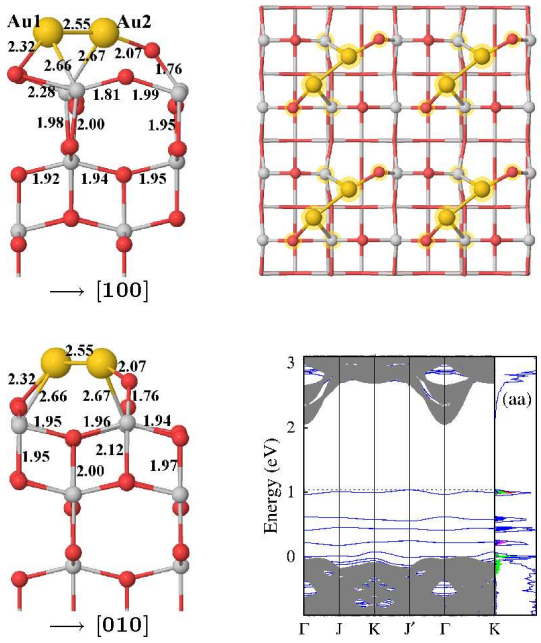

FIG. 3: (color online) Au dimer on anatase TiO_2(001)-2x2 surface (aa-2×2). Side views of the impurity embedded slab model are shown in the left panel where all distances are given in Å. Top view of gold dimers on this surface as well as the corresponding electronic structure are presented on the right panel.

closer reducing the dimer length to 2.55 Å the one at the back row (Au2) pulls the nearest neighbor O1 off its lattice position up by 0.91 Å. However, the O1 in interaction with the Au1 at the first row is elevated by only 0.06 Å. Surprisingly, any geometry that the surface oxygens bonded symmetrically to the dimer is energetically unfavorable.

We also examined the possibility of a dissociative adsorption for various configurations which corresponds to 0.5 ML coverage on this surface. Our results suggest that such a dimer dissociation on the anatase surface is energetically not preferable signifying the strength of Au–Au attraction compared to Au–O and Au–Ti interactions.

Electronically, gold dimer adsorption at 2×2 unit cell drives the anatase (001) surface into a semiconducting state such that it reduces the band gap by 1.04 eV relative to anatase bulk VBM. The impurity band just below the Fermi energy has a minimum at Γ and a maximum at J′ which gives rise to an indirect gap. This otherwise almost flat going state lies higher in energy from a group of five surface-like bands with a separation of 0.34 eV at Γ. It is mainly characterized by Au–Au and Au1–O1 interactions with a partial mixing from the unsaturated surface oxygens. The second defect states disperses conjugately to the first one having a maximum at Γ and a minimum at J′. The surface oxygen that is bonded to Au2 mainly contributes to the second and the third defect states. The next impurity band that has a minimum

at J and a maximum at J′ originates from Au2-O1 bonding. The LDOS of unsaturated O1 ions extend over the VB, also giving partial contribution to all of the defect states.

V. THERMODYNAMIC STABILITY

We analyzed the thermodynamic stability of gold incorporated TiO_2 systems, considered in this work, assuming Au and Ti exchange between the substrate and the surrounding gas phase to account for the formation of substitutional cases.

We assume experimental conditions so that Au is chosen to be in equilibrium with its metallic bulk phase and redefine the zero point of energy at the maximal value of $\mu_{\rm Ti}$ by introducing $\Delta\mu_{\rm Ti} = \mu_{\rm Ti} - \mu_{\rm Ti}^{\rm bulk}$. The relative surface GFEs, $\Delta\gamma$, (or the formation energies) are plotted as a function of $\Delta\mu_{\rm Ti}$ in Fig. 4 over its allowed range of values for 12 surface structures considered in this study. The lower limit for Ti chemical potential has been obtained to be -8.90 eV due to the fact that the surface must keep in thermal equilibrium with the bulk anatase TiO_2 phase.

Our prescription of stability of the phases can predict the structural reconstructions rather than thermally stimulated formations due to the approximation made by omitting the entropy terms in the surface GFE.

The results presented in Fig. 4 suggest that Au incorporation at 1×1 surface is not favorable. For instance, Au substitution for the second layer Ti at 1×1 anatase (001) surface (s2–1×1) is energetically the least preferable phase among the structures considered. Similarly, s1–1×1 case is also thermodynamically unstable. Their formation energies further increase linearly toward Ti–rich experimental conditions. Au adsorption for 1 ML coverage would require an energy of 1.23 eV/1×1 relative to that of the clean surface.

Au interstitials in the 2×2 surface appears to be unfavorable compared to bulk terminated bare anatase TiO_2(001) by the formation energies of 0.44, 0.35 and 0.35 eV/1×1 for c, d, and e cases, respectively. Surprisingly, Au implantation into the interstitial cavities deeper than the fourth atomic layer is slightly more preferable at this surface. These calculated formation energies for Au interstitials in anatase surface are in good agreement with the experimental results of Perkas *et al.*[13]. In an attempt to explain Au induced crystallization (IC) of anatase through gold insertion into TiO_2 which requires thermal treatment at about 80°C by sonication, they stated that Au diffuses into the support layers and forms and intermixed layer through a multiphase diffusion across the gold support interface.

Substitutional gold impurities tend to be linearly more unstable toward Ti-rich conditions. It is also reasonable to see that Au substitution for a second Ti layer cation is energetically more unstable than that for the surface layer Ti over the full range of allowed $\mu_{\rm Ti}$ values. On the other hand, Au(Ti) substitution has been expected to be more preferable in a Ti-poor environment. Indeed, both of the substitutional cases become more stable than the clean relaxed surface under O-rich conditions when the substrate establishes thermodynamic equilibrium with the surrounding oxygen gas phase. Fig. 4 shows that such a surface structure can be realized under the limits, $\Delta\mu_{\rm Ti} < -7.84$ eV and $\Delta\mu_{\rm Ti} < -7.14$ eV for s2 and s1 cases, respectively. Furthermore, Au(Ti) substitution for the surface Ti atom proves to be the most stable phase for $-8.90 < \Delta\mu_{\rm Ti} < -7.98$ eV that corresponds to a Ti-poor environment.

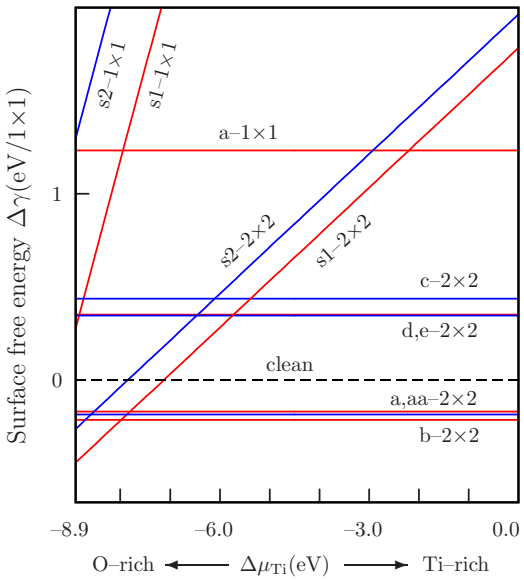

FIG. 4: (color online) Normalized relative surface Gibbs free energies of Au–TiO_2(001)-1×1 and Au–TiO_2(001)-2×2 structures as a function of and over the allowed range of Ti chemical potential. Au impurity ions are chosen to be in thermodynamic equilibrium with *ccp* Au bulk phase.

1ML gold adsorption is not preferable with a formation energy of 1.23 eV relative to that of the clean surface. On the other hand, Au adsorbates at 2×2 unit cell as well as the dimer structure in Fig. 3 happen to be even more stable than the formation of bulk terminated bare (001) surface which is known to be under tensile stress[32] whereby Au bonding causes a lowering of the surface energy by releasing the surface strain[33] We calculated the corresponding relative surface GFEs as -0.17, -0.21 and -0.18 eV/1×1 for a–2×2, b–2×2 and aa–2×2 structures, respectively. Therefore, highly symmetrical structure in Fig. 2(b) appears to be the most stable phase over a wide range of experimental situations within $-7.84 < \Delta\mu_{\rm Ti} < 0$ from Ti-low to Ti-rich equilibrium conditions. However, the differences between the computed GFE values of these three adsorption modes are, surprisingly, not significantly large and can be accepted within the limits of a computational accuracy. In this sense, one cannot conclude that a–2×2 and aa–2×2

are considerably less stable than b–2×2 is. The results rather suggest that these three phases might co-exist in an experimental situation where, interestingly, single Au atom adsorption is metallic while dimer structure is semiconducting. Therefore, overall behavior is expected to be conducting in nature.

VI. CONCLUSIONS

In conclusion, we studied the role of Au mediated lattice relaxations as well as the effect of the impurity itself on the electronic structure of anatase TiO_2(001) for 1×1 and 2×2 surface unit cells. We, additionally, considered gold dimer adsorption on TiO_2(001)-2×2 to account for the strength of Au–Au interaction over Au–O attraction.

In comparison with Ti, due to its spatially wider spread wavefunction, gold maintains a relatively larger distance to the oxygens with which it interacts. In addition, Au exhibits an ample coordination with the neighboring oxygens and, therefore, disturbs local lattice structure. Electronically, an Au adsorbate transfers a limited amount of charge to the nearest neighbor oxygens that reduces the ionicity leading to a relatively weaker impurity–oxygen interaction. On the other hand, Au can attain higher valence charge states in the case of interstitial and substitutional incorporations due to increased coordination number with the neighboring oxygens. For 1ML impurity concentration, gold interstitial enforced local distortion causes significant reconstruction in the form of interlayer segregation due to shortened Au–Au interaction distance. These impurity mediated disturbances derive new defect states and strongly disperse the existing surface bands.

Single Au impurity brings a half-filled impurity state into the band gap of TiO_2(001) which pins the Fermi level leading to metallization, in addition to other filled surface and impurity driven bands within the gap. In the adsorptional and interstitial cases, this state is derived from the CB. For Au interstitials as well as for b–2×2, Fermi energy falls inside the CB. However, substitutional Au makes it up close to the VB also deriving empty impurity states higher in energies toward the CB. The dispersion of the defect states depend on the impurity concentration and the Au–O interaction strength. Therefore, 1×1 cases exhibit the strongest dispersions, and the adsorptional Au incorporations at 2×2 surface lead to flat-like defect states which represent the weakest Au–O interactions.

All Au–incorporated TiO_2(001) structures at 1×1 surface unit cells are unstable. Under strongly oxidizing, Ti–poor conditions gold tends to substitute surface Ti ions at 1/4 ML coverage. On the other hand, for a wide range of experimental situations, from moderate to strongly reducing conditions, Au adsorption is thermodynamically more stable at the 2×2 support surface. Single Au adsorbates at this coverage bring out new acceptor sites as they reduce the surface leading to metallization. Therefore, an additional gold adsorption prefers the dimer structure rather than being dissociative. Gold dimer supported by the slab at 2×2 surface is almost as stable as the single Au adsorption signifying the strength and the role of Au–Au interaction which drives the system into semiconducting regime. Consequently, in an experimental situation which realizes the co-existence of these two phases, the overall behavior is expected to be conducting.

Acknowledgments

EM and ŞE acknowledge financial support from TÜBİTAK, The Scientific and Technological Research Council of Turkey (Grant no: TBAG 107T560). In conjunction with this project, computational resources were provided by ULAKBİM, Turkish Academic Network. & Information Center. OG acknowledges the support of Turkish Academy of Sciences, TÜBA.

[1] S. Kim, S-J. Hwang, and W. Choi, J. Phys. Chem. B **109**, 24260 (2005).
[2] E. Kowalska, H. Remita, C. Colbeau-Justin, J. Hupka, and J. Belloni, J. Phys. Chem. **112**, 1124 (2008).
[3] K. Ko, Y. Lee, and J. Jung, J. Colloid and Interf. Sci. **283**, 482 (2005).
[4] M. Kitano, M. Takeuchi, M. Matsuoka, J. M. Thomas, and M. Anpo, Catal. Today **120**, 133 (2007).
[5] Y. Wang and D. J. Doren, Solid State Commun. **136**, 186 (2005).
[6] E. W. McFarland and J. Tang, Nature **421**, 616 (2003).
[7] I. Marri and S. Ossicini, Solid State Commun., **147**, 205 (2008).
[8] M. S. Chen and W. Goodman, Science **306**, 252 (2004).
[9] J. M. Jung, M. Wang, E. J. Kim, and S. H. Hahn, Vacuum **82**, 827 (2008).
[10] W. Yan, B. Chen, S. M. Mahurin, V. Schwartz, D. R. Mullins, A. R. Lupini, S. J. Pennycook, S. Dai, and S. H. Overbury, J. Phys. Chem. B **109**, 10676 (2005).
[11] J. Li and H. C. Zeng, Chem. Mater. **18**, 4270 (2006).
[12] A. Grirane, A. Coma, H. Garcia, Science **322**, 1661 (2008).
[13] N. Perkas, V. G. Pol, S. V. Pol, and A. Gedanken, Crystal Growth & Design, **6**, 293 (2006).
[14] R. Hengerer, B. Bolliger, M. Erbudak, and M. Grätzel, Surf. Sci. **460**, 162 (2000).
[15] A. Bouzoubaa, A. Markovits, M. Calatayud, and C. Minot, Surf. Sci. **583**, 107 (2005).
[16] A. G. Thomas, W. R. Flavell, A. K. Mallick, A. R. Kumarasinghe, D. Tsoutsou, N. Khan, C. Chatwin, S. Rayner, G. C. Smith, R. L. Stockbauer, S. Warren, T. K. Johal, S. Patel, D. Holland, A. Taleb, and F. Wiame, Phys. Rev. B **75**, 035105 (2007).
[17] S. Munnix and M. Schmeits, Phys. Rev. B **30**, 2202 (1984).
[18] A. Beltrán, J. R. Sambrano, M. Calatayud, F. R. Sensato, and J. Andrés, Surf. Sci. **490**, 116 (2001).
[19] M. Lazzeri, A. Vittadini, and A. Selloni, Phys. Rev. B **63**,

155409 (2001).
[20] M. Calatayud and C. Minot, Surf. Sci. **552**, 169 (2004).
[21] J. P. Perdew, K. Burke, and M. Ernzerhof, Phys. Rev. Lett. **77**, 3865 (1996).
[22] P. E. Blöchl, Phys. Rev. B **50**, 17953 (1994).
[23] G. Kresse and D. Joubert, Phys. Rev. B **59**, 1758 (1999).
[24] G. Kresse and J. Hafner, Phys. Rev. B **47**, 558 (1993).
[25] G.-X. Qian, R. M. Martin, and D. J. Chadi, Phys. Rev. B **38**, 7649 (1988).
[26] K. Reuter and M. Scheffler, Phys. Rev. B **65**, 035406 (2001).
[27] B. Meyer, Phys. Rev. B **69**, 045416 (2004).
[28] V. Timon, S. Brand, S. J. Clark, M. C. Gibson, and R. A. Abraham, Phys. Rev. B **72**, 035327 (2005).
[29] E. Mete, D. Uner, O. Gülseren, and Ş. Ellialtıoğlu, Phys. Rev. B **79**, 125418 (2009).
[30] E. Sanville, S. D. Kenny, R. Smith, and G. Henkelman, J. Comp. Chem. **28**, 899 (2007).
[31] M. Calatayud, P. Mori-Sánchez, A. Beltrán, A. Martín Pendás, E. Francisco, J. Andrés, and J. M. Recio, Phys. Rev. B **64**, 184113 (2001).
[32] M. Lazzeri and A. Selloni, Phys. Rev. Lett. **87**, 266105 (2001).
[33] A. Vittadini and A. Selloni, J. Chem. Phys. **117**, 353 (2002).